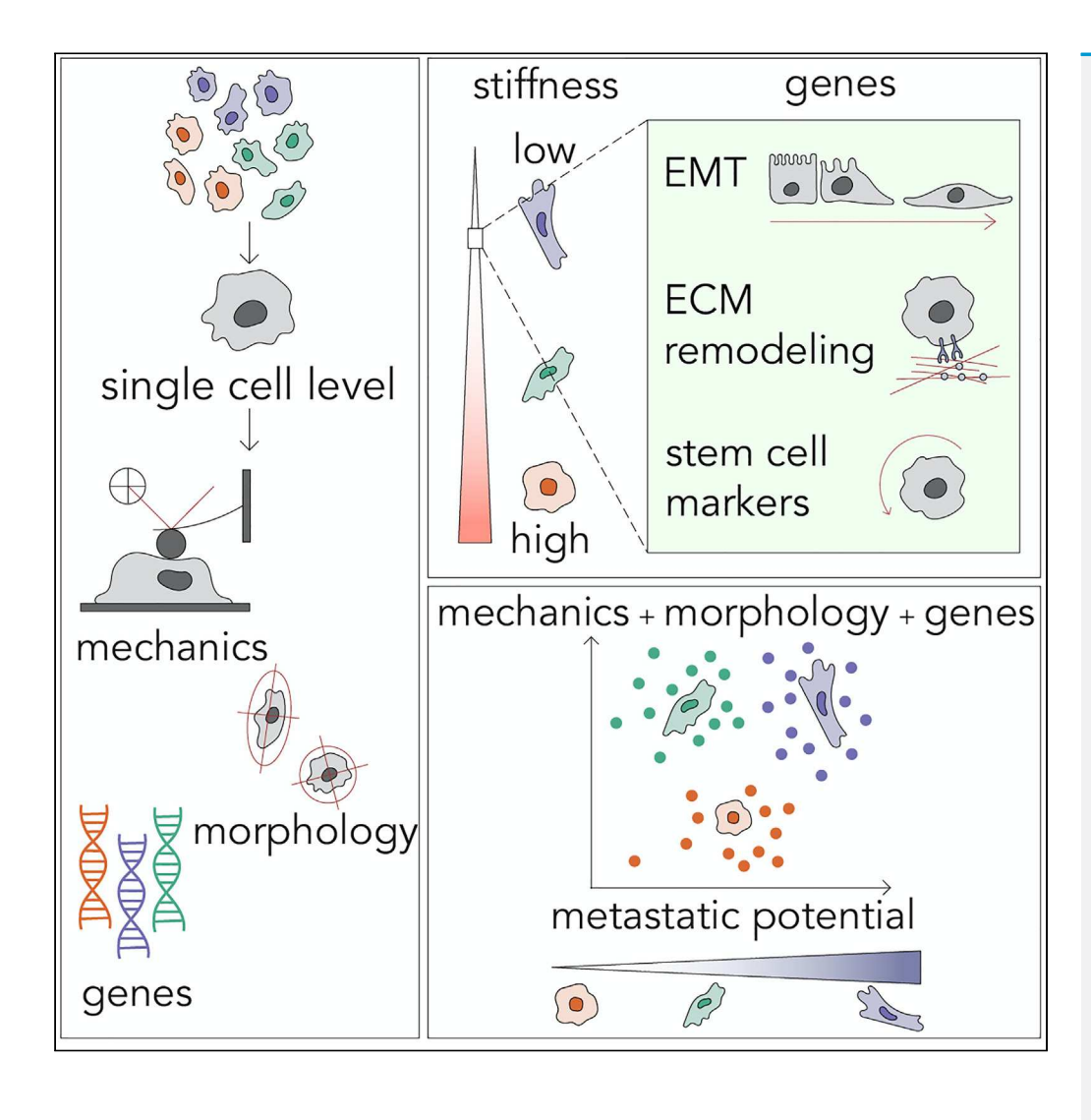
iScience



Article

Correlating mechanical and gene expression data on the single cell level to investigate metastatic phenotypes



Katherine M.
Young, Congmin
Xu, Kelly Ahkee,
..., John F.
McDonald, Peng
Qiu, Todd Sulchek

todd.sulchek@me.gatech.edu

Highlights

Method to correlate mechanics, morphology, and gene expression data of single cells

Pro-metastatic gene expression pattern is associated with soft single

Stiffness correlates more highly with metastatic programs than cytoskeletal genes

Gene expression combined with mechanics data separates cells by metastatic ability

Young et al., iScience 26, 106393 April 21, 2023 © 2023 The Author(s). https://doi.org/10.1016/ j.isci.2023.106393

iScience



Article

Correlating mechanical and gene expression data on the single cell level to investigate metastatic phenotypes

Katherine M. Young,¹ Congmin Xu,¹ Kelly Ahkee,¹ Roman Mezencev,² Steven P. Swingle,³ Tong Yu,¹ Ava Paikeday,¹ Cathy Kim,¹ John F. McDonald,² Peng Qiu,¹ and Todd Sulchek^{1,3,4,*}

SUMMARY

Stiffness has been observed to decrease for many cancer cell types as their metastatic potential increases. Although cell mechanics and metastatic potential are related, the underlying molecular factors associated with these phenotypes remain unknown. Therefore, we have developed a workflow to measure the mechanical properties and gene expression of single cells that is used to generate large linked-datasets. The process combines atomic force microscopy to measure the mechanics of individual cells with multiplexed RT-qPCR gene expression analysis on the same single cells. Surprisingly, the genes that most strongly correlated with mechanical properties were not cytoskeletal, but rather were markers of extracellular matrix remodeling, epithelial-to-mesenchymal transition, cell adhesion, and cancer stemness. In addition, dimensionality reduction analysis showed that cell clustering was improved by combining mechanical and gene expression data types. The single cell genomechanics method demonstrates how single cell studies can identify molecular drivers that could affect the biophysical processes underpinning metastasis.

INTRODUCTION

Metastasis is the cause of 90% of cancer-related deaths.¹ The metastatic cascade is a multi-step process that allows tumor cells to undergo epithelial-to-mesenchymal transition (EMT), dissociate from the tumor, degrade the extracellular matrix (ECM), migrate to neighboring tissues and undergo mesenchymal-to-epithelial transition (MET) to form a new metastatic tumor. For cancer cells to invade and migrate, their mechanical properties often change. The processes of EMT and MET reorganize the cytoskeleton and allow for cell motility.^{2,3} Cancer cell softening has been observed in many cancer types^{3,4}; more specifically, as metastatic potential increases, cell stiffness decreases.^{4–7} However, we lack a full understanding of how molecular pathways are related to these mechanical phenotypes. Such knowledge may unlock potential control points in these pathways to determine how cells respond to therapeutic agents and to understand how mechanics can be used as diagnostic biomarkers.

The advent of single cell analysis has been critical to understand the heterogeneity of cellular mechanisms of disease. When studying whole populations of cells, responses from subsets of cells are lost because of the averaging of genetic expression. In contrast, single cell methods allow for the targeted observation of gene expression in single cells within a heterogeneous population. However, gene expression measurements alone do not fully describe complex cellular processes, including the various processes in metastasis. In fact, a poor correlation between mRNA measurements and protein content in cells is often observed. The this reason, the study of single cells using multiple modalities can better connect cell properties with function. To this end, methods have been developed to link transcriptome level data with epigenomic regulation and proteomic expression on the single cell level. Moreover, new methods can specifically link single cell transcriptional profiles with cell size, morphology and electrophysiology. However, there has not been a study linking single cell mechanics and gene expression, as needed to understand the biomechanical aspects of metastasis.

Here we describe the first method of its kind to combine mechanical, morphological, and gene expression data from individual cells to link molecular and biophysical processes in metastasis. Single cell RT-qPCR

¹Wallace H. Coulter Department of Biomedical Engineering, Georgia Institute of Technology, 313 Ferst Drive, Atlanta, GA 30332-0535, USA

²School of Biology, Georgia Institute of Technology, 313 Ferst Drive, Atlanta, GA 30332-0405, USA

³George W. Woodruff School of Mechanical Engineering, Georgia Institute of Technology, 801 Ferst Drive, Atlanta, GA 30332-0405, USA

⁴Lead contact

*Correspondence: todd.sulchek@me.gatech.edu

https://doi.org/10.1016/j.isci. 2023.106393







data, single cell mechanical measurements from atomic force microscopy (AFM), and morphological measurements obtained by optical microscopy were used to study three ovarian cancer cell lines of varying metastatic potential. We identified several genes related to the metastatic process that are significantly correlated with cell mechanics. We find the migratory and invasive ability of cells are linked to mechanical and morphological markers as strongly as sets of molecular readouts, resulting in more effective clustering by the metastatic potential of cells. This understanding of mechanical properties and metastatic pathways can lead to the discovery of new diagnostic biomarkers and therapeutic targets that may benefit the identification and treatment of invasive cancers.

RESULTS

Single cell genomechanics method combines AFM and targeted RT-qPCR

The single cell genomechanics method was developed to collect mechanical, morphological, and gene expression data for individual cells. Cells were cultured on a gridded coverslip that was used to track the location of each cell throughout AFM measurements, optical imaging, and subsequent micropipette isolation for gene expression analysis (Figure 1A). Optical images of each cell were analyzed using ImageJ software and elliptical fitting to determine morphological properties, including cell size, aspect ratio, circularity, roundness, and solidity (Figure 1B). AFM cell indentation force curves were conducted to measure the Young's modulus and viscous relaxation time constants for each cell using a Hertzian contact mechanics model (Figure 1C) and Zener model of cell viscoelasticity (Figure 1D), respectively. After mechanical probing, each cell was located using the gridded substrate as registry and isolated with a micropipette, using negative pressure aspiration (Video S1) and positive pressure to deposit the cell into a tube for immediate lysis and preparation for gene expression analysis. This analysis was conducted with the Fluidigm BioMark 96.96 Dynamic Array integrated fluidic chip to perform RTqPCR of 96 genes in 96 cells per chip. The genes tested include those associated with EMT, metastatic enhancers and suppressors, cancer stemness, extracellular matrix remodeling, cytoskeletal remodeling, cancer malignancy, and multiple growth signaling pathways as classified by the PANTHER Classification System (http://www. pantherdb.org) (Figure 1E and Table S1). For our investigation, we used three model ovarian cancer cell lines of varying metastatic potential. OVCAR3 is an epithelial cell line that represents serous adenocarcinoma, HEY is a mesenchymal cell line that represents serous carcinoma, and HEY A8 is a derivative cell line of HEY that is more metastatic and mesenchymal. 16

We used custom R code (see STAR Methods) to automate the process of extracting the cell's Young's modulus and viscous time constants from multiple AFM force curves at once (282 force curves, one per cell). The validation of this code is provided in Figures S1A and S1B comparing the analysis of cell stiffness measurements extracted automatically to those extracted manually using commercial software at low (10–50%) indentation. We found that the epithelial OVCAR3 cells are statistically stiffer than the mesenchymal HEY and HEY A8 cell types (p < 0.05, Tukey's HSD post-hoc test). To confirm that the cell mechanical measurements were not biased by the amount of time the cells were out of the incubator, we compared the cell measurement number (a proxy for time of the experiment), to the cell stiffness (Figure S1C). We found there was no significant correlation between cell measurement number and cell stiffness for any of the cell types (p > 0.1, t-test for significance of Pearson's correlation test).

The morphology analysis confirms the epithelial and mesenchymal status for each cell type. The epithelial cell line, OVCAR3, had shorter major axes with aspect ratios close to 1 whereas the mesenchymal cells HEY and HEY A8 were more elongated with elevated aspect ratios (Figures S1E and S1F). In addition, OVCAR3 cells were more circular than HEY cells which were more circular than HEY A8 cells (Figure S1G). Finally, the measure of solidity was used to compare the number of protrusions from each cell, with HEY A8 cells being the least solid and with the most protrusions, whereas OVCAR3 cells were the most solid (Figure S1H). Representative images of each cell type are included for comparison (Figure S1D).

To confirm the isolation of single cells without affecting gene expression, we plotted the normalized expression of each cell isolated through micropipette aspiration and compared the expression distribution to the normalized bulk expression of each gene for each cell type (Figure S2). We found that for all cell types the normalized gene expression was significantly correlated between the average single cell expression and the population measurement (p < 1E-5, HEY A8 cor = 0.557, HEY cor = 0.445, OVCAR3 cor = 0.627), supporting our hypothesis that the isolation method had little effect on gene expression (Figure 2A). Importantly, we observed the population measurement of the average expression of the cells (represented as a point in the violin plot) does not represent the true expression of many actual single cells (Figures 2B,



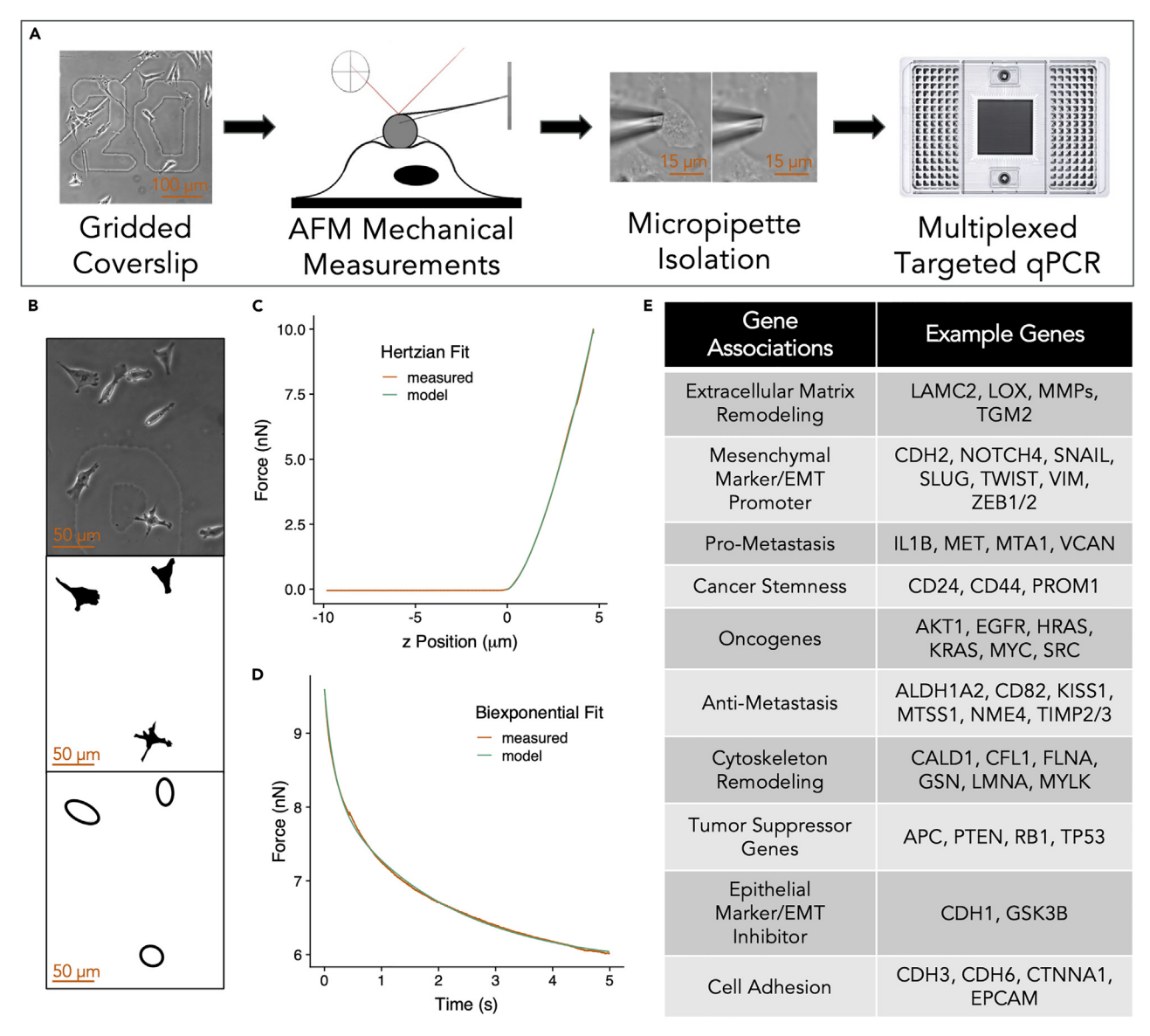


Figure 1. Development of new method to combine single cell morphological, mechanical, and gene expression data

(A) Schematic describing the process to collect three types of data for each single cell in which cells are grown on a gridded coverslip, atomic force microscopy is used to measure cell's Young's modulus and viscous properties, a micropipette is used to aspirate and isolate each probed cell, and a Fluidigm integrated fluidic chip is used for multiplexed targeted qPCR to measure the gene expression of 96 genes. Scale bars represent 100 μ m and 15 μ m as notated.

- (B) Cell morphological parameters are extracted from images of cells on the gridded coverslip, each fit with an ellipse to help determine cell size, aspect ratio, circularity, roundness, and solidity. Scale bars represent $50 \mu m$.
- (C) Each AFM force curve was fit using an equation defined by Hertzian contact mechanics to identify each cell's Young's modulus.
- (D) Each dwell portion of the AFM force curve was fit using a biexponential equation to identify each cell's fast and slow time viscous time constants.
- (E) A partial list of genes of interest to investigate the relationship between cell mechanics, gene expression, and metastatic potential.

2C, 2E, and 2F). In addition, the population measurement does not accurately capture the heterogeneity and sometimes bimodal distribution of single cell gene expression, sometimes representing the expression of the subset of cells with high expression, without accurately describing a large portion of low expressing cells (Figure 2D).

To further confirm the lack of change in single cell gene expression because of micropipette aspiration, we compared the gene expression of cells collected by aspiration to those of cells isolated using



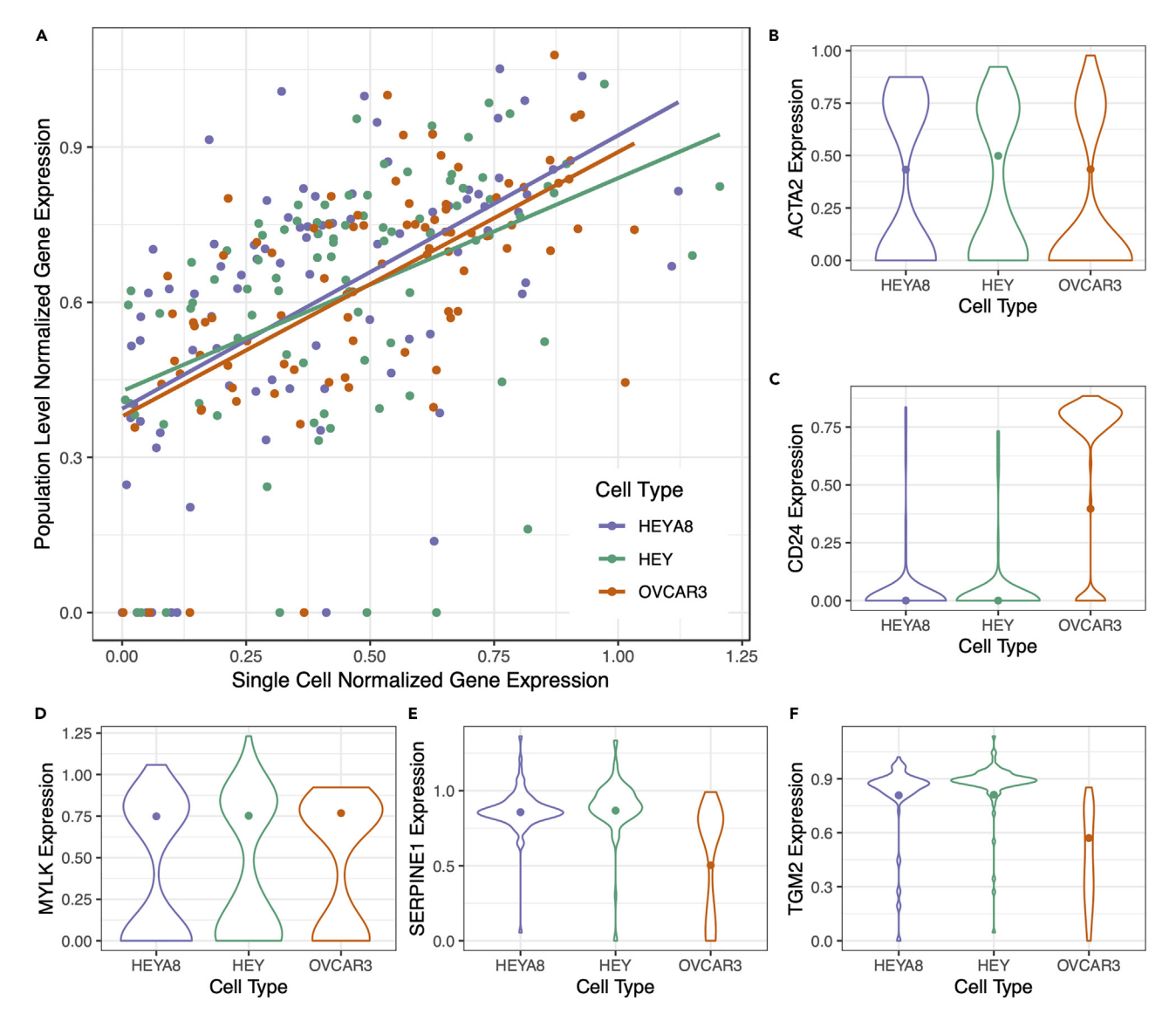


Figure 2. Population versus Single Cell Gene Expression

(A) Comparison of population level normalized gene expression and average single cell normalized gene expression. Each point represents the expression of a particular gene in a cell type, 88 genes total per cell type. Population level data was gathered using RT-qPCR of purified RNA from a flask of each cell type whereas single cell data is the mean expression of a gene across all single cells from each cell type. For all cell types, the normalized gene expression was significantly correlated between the average single cell expression and the population measurement (p < 1E-5, HEY A8 cor = 0.557, HEY cor = 0.445, OVCAR3 cor = 0.627).

(B–F) Violin plots of the distribution of single cell data for each cell type. The datum point in the middle of each violin plot represents the population level expression level collected using RT-qPCR with bulk RNA for ACTA2 (B), CD24 (C), MYLK (D), SERPINE1 (E) and TGM2 (F).

fluorescence-activated cell sorting (FACS). (Figure S3A). The average expression between the two groups of cells was significantly correlated (cor = 0.887, p < 1E-15), implying little effect of collection method on gene expression (Figure S3B). Micropipette aspiration, however, resulted in a higher efficiency of gene expression data collected, with 277 of 282 (98.227%) micropipette-isolated cells having measurable gene expression data whereas only 40 of 94 (42.553%) FACS isolated cells produced measurable data (Figure S3C). Finally, primer designs were collected from literature and validated to amplify the expected product (Table S2). With this validation, the genomechanical method represents the first process for linking mechanical and imaging data with gene expression data on the single cell level.





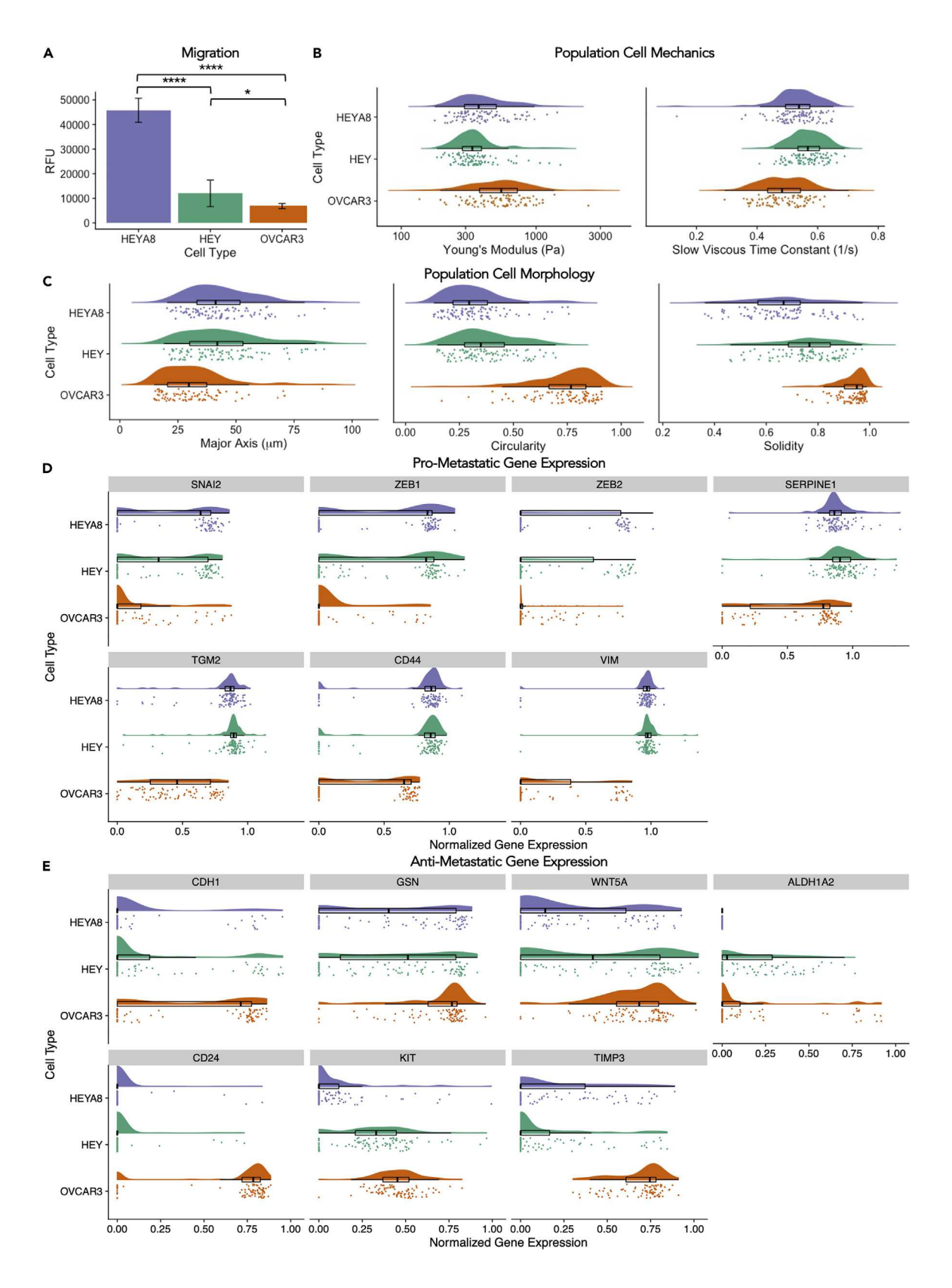






Figure 3. Comparison of population behavior of HEY A8, HEY and OVCAR3 cell lines

(A) Transwell migration assay data demonstrate the increased migratory ability of the HEY A8 cells compared to the HEY cells (Tukey's HSD, ****, p < 0.0001). The epithelial OVCAR3 cells are the least migratory (HEYA8 versus OVCAR3, Tukey's HSD, ****, p < 0.0001, HEY versus OVCAR3, Tukey's HSD, *, p < 0.005). Cells that migrated through the 8 micron Transwell were fluorescently quantified; RFU is relative fluorescent units.

(B) The epithelial cell line OVCAR3 is on average stiffer with a reduced slow viscous time constant when compared with the mesenchymal HEY and HEY A8 cell lines.

(C) With increasing migratory ability, we see a trend of increasing cell elongation (increased major axis and reduced circularity) and cell protrusions (reduced solidity).

(D) With increasing migratory ability, we see a trend of increasing expression of EMT-driving transcription factors (SNAI2, ZEB1, ZEB2), ECM remodeling proteins (SERPINE1, TGM2), cancer stemness (CD44) and mesenchymal markers (VIM).

(E) With increasing migratory ability, we see a trend of decreasing expression of epithelial markers (CDH1), metastasis suppressors (GSN, WNT5A, ALDH1A2), cell differentiation markers (CD24, KIT), and ECM remodeling inhibitors (TIMP3). Raincloud plots consist of an overlay of a half violin plot, a boxplot depicting summary statistics for each population as well as a jitter plot displaying single cell values.

Population level measurements insufficient to distinguish between cell types

At the population level, we observe several mechanotypic, genotypic, and phenotypic trends between the three ovarian cancer cell types. HEY A8 cells are the most migratory, whereas the OVCAR3 cells are least migratory (Figure 3A). Both the mesenchymal HEY and HEY A8 cells are significantly softer than the epithelial OVCAR3 cells. In addition, we observed OVCAR3 cells exhibit a reduced viscous time constant meaning they relax more slowly and are more viscous (Figure 3B). Comparing the morphological measurements of each cell type, increased migration at the population level correlated with increased cell elongation (demonstrated by increased major axis and reduced circularity) and cell protrusions (measured by reduced solidity) (Figure 3C). From an analysis of all genes of interest (Figure S4), increasing migration at the population level correlated with increased gene expression associated with pro-metastatic processes, including EMT-driving transcription factors, ECM remodeling proteins, cancer stemness and mesenchymal markers (Figure 3D), such as SNAI2, TGM2, and VIM. Also increasing migratory ability at the population level correlates with decreased gene expression associated with anti-metastatic processes, including epithelial markers, metastasis suppressors, cell differentiation markers and ECM remodeling inhibitors (Figure 3E), such as CDH1, GSN, and KIT. These population level trends support the existence of correlation between cancer cell mechanotype, genotype, and phenotype. However, we note there is substantial overlap between these parameters for the different cell types that preclude drawing accurate connections between cell morphology, mechanics, and genetic expression. Thus, single cell measurements are needed, even within these nominally uniform cell lines because of the heterogeneity of expression profiles, to determine how cell mechanics and gene expression work together during metastatic processes.

Pro-metastatic gene expression pattern associated with soft single cells

We examined the single cell correlations between gene expression and cell mechanical properties of 282 ovarian cancer cells (92 HEY A8 cells, 100 HEY cells, and 90 OVCAR3 cells). After initial quality control checking for stable expression of housekeeping genes, we removed 9 cells, resulting in 273 cells for analysis (91 HEY A8 cells, 95 HEY cells, 87 OVCAR3 cells). A Spearman's rank correlations analysis found 41 genes that were significantly correlated with cell stiffness (p < 0.05) (Figure 4A). Of the 14 genes negatively correlated with stiffness, 11 genes were associated with pro-metastatic functions, such as extracellular remodeling, mesenchymal markers, cancer stemness, and oncogenic behavior (Figure 4B, Table S3). Meanwhile, 17 of the 25 positively correlated genes are related to anti-metastatic functions, such as cell adhesion, epithelial markers, tumor and metastasis suppression and cytoskeletal proteins.

Counterintuitively, the genes that are most highly correlated with cell stiffness are not directly related to the cytoskeleton, but rather drive various processes important for promoting or preventing metastasis. The gene most strongly negatively correlated with cell stiffness is TGM2 which codes for transglutaminase 2, an ECM remodeling protein. The gene most strongly positively correlated with cell stiffness is SRC, an oncogene that has been associated with stress fiber assembly and increased proliferation. siRNA was used to knockdown the expression of TGM2 and SRC in the mesenchymal HEY A8 and epithelial OVCAR3 cell lines. Because siRNA targets genes through mRNA degradation and because our original data showed a correlation between cell stiffness and gene transcript quantity, we confirmed the knockdown of each gene of interest at the transcript level using RT-qPCR (48.9% and 98.9% reduction in TGM2 expression and 86.0% and 84.9% reduction in SRC expression in the OVCAR3 and HEY A8 cells respectively) (Figures S5A-S5D). After knocking down TGM2, we observed a statistically significant increase in the stiffness of OVCAR3 cells as expected, although there was not a significant change in stiffness



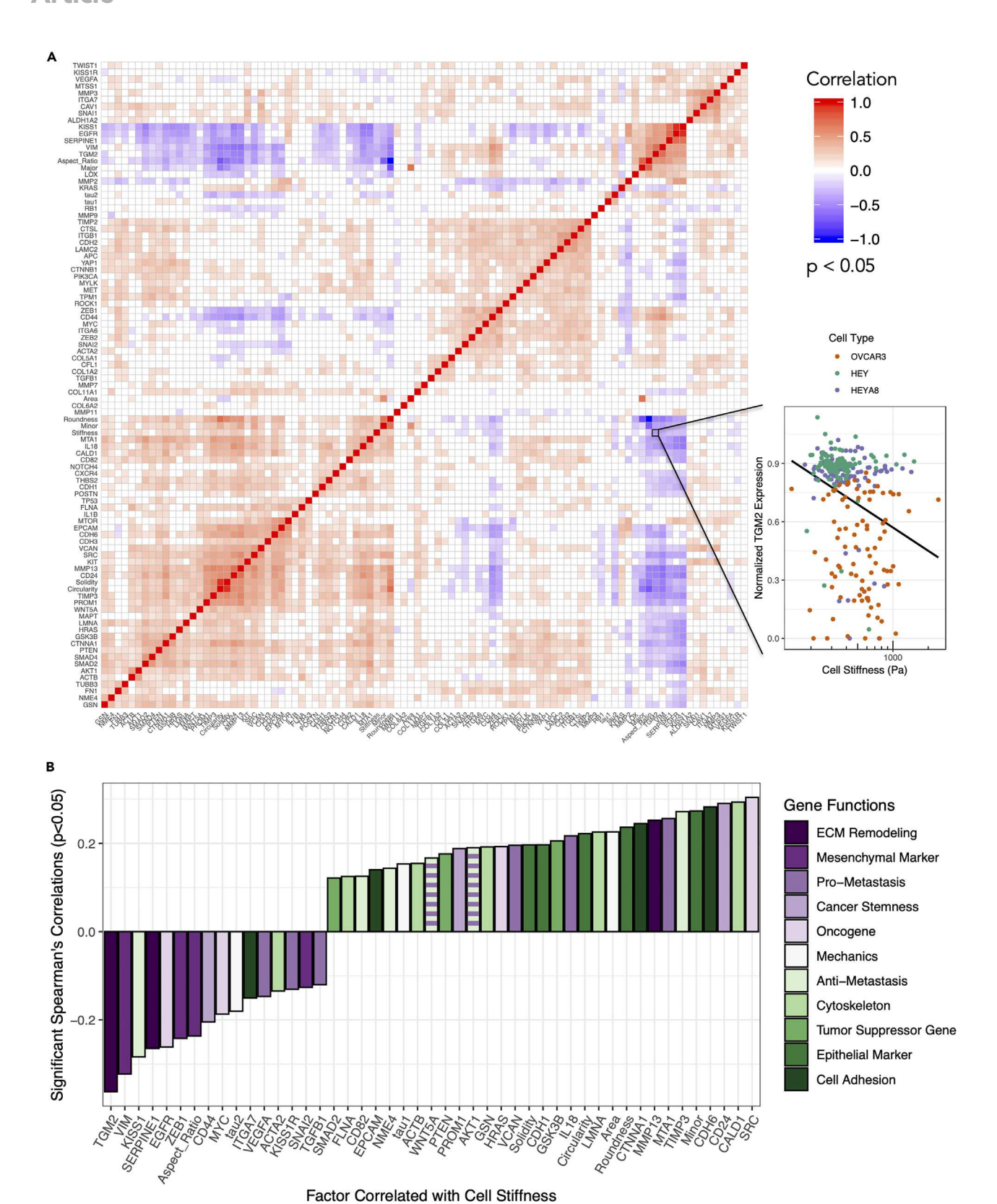






Figure 4. Single cell correlations between genetic, morphological, and mechanical parameters

(A) Correlation matrix comparing the Spearman's pairwise correlations between each combination of single cell genetic, morphologic, and mechanical data. Only statistically significant (p < 0.05) correlations are plotted. The inset shows the single cell values for cell stiffness and normalized TGM2 expression. (B) Significant correlations between cell stiffness and genetic, morphological, and mechanical parameters. Bars are colored by nominal function. Data can be explored further with interactive plots at https://kyoung74.github.io/PlotlyPlots/.

for HEY A8 cells with the same knockdown (Figures S5E and S5F). Of interest, *TGM2* is more highly expressed in HEY A8 cells (Figure S2), but the significant effect was observed in the OVCAR3 cells. After knocking down *SRC*, we observed a statistically significant decrease in stiffness of HEY A8 cells as expected, although not a significant change in stiffness for OVCAR3 cells with the same knockdown (Figures S5E and S5F). Similarly to the *TGM2* data, *SRC* is more highly expressed in the OVCAR3 cells when observed at the single cell level (Figure S2), but the significant effect was observed in the HEY A8 cells. In addition to confirming the correlations of some of these genes of interest with cell stiffness, this data demonstrates interesting cell type specific behaviors that may be related to the initial cell state of each of these cell types of different epithelial and mesenchymal status. We also repeated the correlation analysis for the three cell types separately. From this analysis, we were able to identify additional cell type specific correlations between genes of interest and cell stiffness (Figures S6A–S6C).

Single data type measurements insufficient to distinguish between cell types

Principal component analysis (PCA) was used to reduce the dimensionality of the gene, morphologic, and mechanical data separately to group cells into clusters associated with a cell type and, by proxy, metastatic potential. Surprisingly, the use of single cell expression of 85 genes was insufficient to effectively separate by cell type (Figure 5A). We found that morphological (Figure 5B) and mechanical data (Figure 5C) alone were also inadequate to separate by cell type. We quantified the success of each PCA clustering scheme using the Davies-Bouldin (DB) index (see STAR Methods) (Figure 5H). A lower DB index represents a lower ratio of intra-cluster to inter-cluster variation and a more optimal clustering scheme. We found that the low inter-cluster variation between the HEY and HEY A8 populations, which were derived from the same cell line with different migratory potential, dominated the DB index and resulted in poor clustering of cell types when only considering gene expression. Thus, a single data type is insufficient to classify closely related HEY and HEY A8 cell types that differ in metastatic potential.

Combining gene expression, mechanical and morphological data types improves cell type clustering

The DB index for cell clustering is substantially improved (that is reduced) by combining the gene expression, morphological, and mechanical data collected for each single cell using partial least squares (PLS) analysis (see STAR Methods). Combining the morphological and mechanical data reduces the DB index below that of gene expression data alone showing that using multiple data types to cluster cells is more effective than using a single data type (Figure 5D). Cell clustering was further improved through the combinations of gene expression data with imaging data (Figure 5E) and with mechanical data (Figure 5F), providing superior clustering, surpassing a conservative assessment of an optimal DB index 17 (Figure 5H). Distinguishing between the closely related HEY and HEY A8 populations was seen only when all three data types were combined (Figure 5G), which demonstrates the ability to cluster cells based on their metastatic potential.

DISCUSSION

This study has identified several genes that are significantly correlated with cell mechanical properties. Of particular interest include negative correlations between cell stiffness and *TGM2*, a crosslinking protein involved with ECM remodeling and EMT in ovarian cancer, ¹⁸ the intermediate filament protein vimentin, a mesenchymal marker and mediator of cytoskeletal organization, ¹⁹ and *ZEB1*, a transcription factor implicated in the EMT and metastatic processes. ²⁰ *TGM2* crosslinks collagen, stiffening the matrix around cells resulting in changes to their contractile and proliferative responses. ^{21,22} Of interest, increased matrix stiffness has also been associated with induction of the EMT process through the TWIST1-G3BP2 mechanotransduction pathway, ²³ possibly relating increased *TGM2* expression to a softer cell mechanotype and mesenchymal phenotype through its mechanism of stiffening the surrounding microenvironment. This connection is further supported by our experimental validation of *TGM2* knockdown and the increase of cell stiffness in the OVCAR3 cell type. These negatively correlated genes related to ECM remodeling and a more mesenchymal phenotype support an association of a softer phenotype with more migratory,





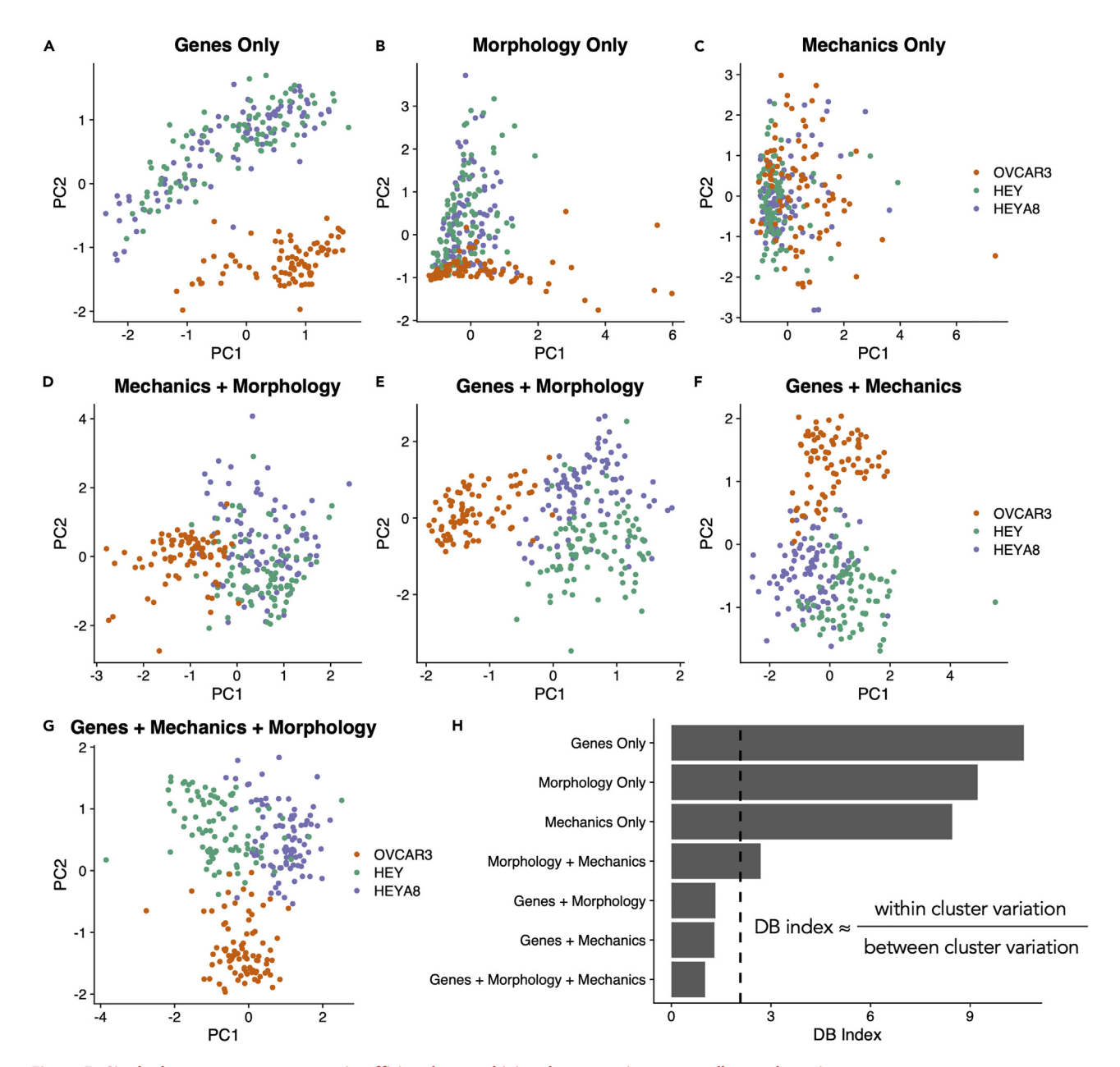


Figure 5. Single data type measurements insufficient but combining data types improves cell type clustering

PCA cell clustering with single data type using single cell gene expression (A), morphological parameters (B) or mechanical parameters (C). (D) PCA clustering using both morphological and mechanical data.

- (E) PCA clustering using both morphological and genetic data.
- (F) PCA clustering using both genetic and mechanical data.
- (G) PCA clustering using all three data types, genetic, morphological, and mechanical data.
- (H) Comparison of the Davies–Bouldin index for each clustering pattern, which is a ratio of within-cluster variation and between-cluster variation. Thus, a minimized DB index is associated with a more optimal clustering scheme. The dashed line refers to a conservative optimal value of the DB index.¹⁷

metastatic behavior. This claim is further supported by other work that identifies a positive relationship between cell deformability (which is inversely related to cell stiffness) and a mesenchymal state. ^{24,25}

Of note from the positive correlations are the metastasis suppressor and metalloproteinase inhibitor TIMP3, nuclear structure protein lamin A, which protects against DNA damage and provides a major barrier to cell invasion 26 and E Cadherin, an adhesion protein and epithelial marker, implying a relationship





between stiffer cells and a more epithelial and less migratory phenotype. In addition, there are positive correlations between stiffness and *SRC*, an oncogene that causes increased cell stiffness through increase in stress fiber assembly and focal adhesion formation, ²⁷ which we experimentally demonstrated knockdown of results in cell softening in the HEY A8 cell type, and *AKT1*, an oncogene that has been associated with both metastasis promotion and suppression. ²⁸ The associations of increased stiffness with genes related to proliferation and an epithelial-like state could support a dichotomy between a cells' abilities to proliferate and to migrate, known as the "go or grow" hypothesis. ²⁹ For example, during collective cell migration, phenotypic differences result in leader and follower tumor cell subpopulations in which leader cells are highly migratory with lower proliferative ability and follower cells represent the converse. ³⁰ Further work examining the mechanics of these leader and follower subpopulations could elucidate the relationship between cell stiffness, proliferation, and migration states. In addition, recent work has confirmed the correlation of E-cadherin expression in cells with a weakly migratory phenotype; however, they interestingly identified these cells as more metastatic which brings up the question of dissecting the role of cell mechanics on the separate processes of cell migration and the multi-step metastatic cascade ³¹

In the future, this method could also be applied to other cancer types and dissociated primary tumor cells as well as to other biological problems where cellular mechanics can play a role in differences between normal and diseased state, including chemoresistance, angiogenesis, and stem cell differentiation. 32-35 Although this study has focused on the role of cellular mechanics in the context of cancer and metastasis, because the cytoskeletal makeup and motility machinery is conserved across cell types, we expect that this method could be used to investigate the relationship between mechanotype with motility phenotypes in both diseased and healthy tissues.

With this new genomechanical method we have explored important connections between a cell's mechanotype, genotype, and phenotype. Studying cells at a single cell level has allowed us to form new hypotheses about the association of a mesenchymal phenotype and soft mechanotype with ECM remodeling pathways and epithelial and proliferative phenotypes with a stiff mechanotype as well as draw conclusions about the molecular factors associated with the metastatic process. Because of the use of our technique, we have produced an extremely rich dataset that can be explored further to understand inter- and intra-cell line variability and the various gene networks that may be governing a single cell's metastatic potential.

Limitations of the study

These studies represent the first exploration of combining cell mechanical data and gene expression data at the single cell level. While starting to gain a mechanistic understanding of the mechanical regulation of the metastatic process, we do recognize several limitations to our current study as well as potential future lines of experimentation. Our current work to validate this new method focused on the use of cancer cell lines grown on unphysiologically rigid glass and tissue culture plastics. To improve the translatability of the work, the method could be applied to additional ovarian cancer cell lines and other cancer types, dissociated primary tumor cells, or collected circulating tumor cells attached to tissue-stiffness-matched hydrogels or decellularized tissue matrix, although that soft substrate would need to be accounted for during AFM mechanical measurements. In addition, the current method could be expanded from targeted RT-qPCR to single cell RNA sequencing, using a system such as SmartSeq2, to broaden the scope of the genes explored, as we are certain there are other interesting relationships between a cell's genotype, mechanotype, and phenotype that we have not yet observed. Finally, as noted above, metastasis is a multi-step process that often relies on collective action of multiple tumor cells to successfully colonize a metastatic site. Our study explores the intrinsic properties of single cells, but we recognize that cell migration and metastasis also involves important interactions between multiple cells and their environment, which is beyond the scope of this study and this method.

STAR*METHODS

Detailed methods are provided in the online version of this paper and include the following:

- KEY RESOURCES TABLE
- RESOURCE AVAILABILITY
 - O Lead contact
 - O Materials availability
 - O Data and code availability
- EXPERIMENTAL MODEL AND SUBJECT DETAILS



- Ovarian cell culture and sample preparation
- METHOD DETAILS
 - AFM and force curve analysis
 - O Image analysis
 - Micropipette isolation
 - O Fluorescent activated cell sorting (FACS)
 - O Primer design and validation
 - Fluidigm targeted qPCR
 - O Population gene expression qPCR
 - Migration assay
 - O siRNA transfection
- QUANTIFICATION AND STATISTICAL ANALYSIS
 - O PCA and PLS cell clustering analysis
 - O Correlation analysis

SUPPLEMENTAL INFORMATION

Supplemental information can be found online at https://doi.org/10.1016/j.isci.2023.106393.

ACKNOWLEDGMENTS

The authors would like to thank Ilya Kolb, Corey Landry, and Mighten Yip for help with micropipette aspiration; Nicholas Stone for help with code written to analyze AFM force curves; Dalia Arafat and the Institute for Bioengineering and Biosciences Core Facilities for help with gene expression analysis; and Chelsea Mariano for her design of the graphical abstract. This research project was supported by funding through the National Science Foundation, award #1538161 and award #2225476, and through the National Institutes of Health: National Cancer Institute, grant #1F31CA243345-01.

AUTHOR CONTRIBUTIONS

K.M.Y. contributed to the design of the work, the acquisition, analysis and interpretation of data, the creation of new software used in the work, funding acquisition, and wrote the manuscript. C.X. contributed to the analysis and interpretation of the PCA clustering and DB index analysis. K.A. contributed to the acquisition of the primer validation and morphology data. S.S., T.Y., A.P., and C.K. contributed to the acquisition and analysis of the siRNA validation of the effect of *TGM2* and *SRC* on cell stiffness. R.M., J.M., P.Q., and T.S. contributed to the design of the work. T.S. was also responsible for the conception of the work, funding acquisition, supervision, and substantially revised the manuscript. All authors read and approved the final manuscript.

DECLARATION OF INTERESTS

The authors declare no competing interest.

Received: October 1, 2021 Revised: November 9, 2022 Accepted: March 7, 2023 Published: March 13, 2023

REFERENCES

- Mehlen, P., and Puisieux, A. (2006). Metastasis: a question of life or death. Nat. Rev. Cancer 6, 449–458. https://doi.org/10. 1038/nrc1886.
- Shankar, J., and Nabi, I.R. (2015). Actin cytoskeleton regulation of epithelial mesenchymal transition in metastatic cancer cells. PLoS One 10, e0119954. https://doi. org/10.1371/journal.pone.0119954.
- 3. Rianna, C., and Radmacher, M. (2016). Cell mechanics as a marker for diseases: biomedical applications of AFM. In AIP

- Conference Proceedings (AIP Publishing), p. 020057. https://doi.org/10.1063/1.4960276.
- Guck, J., Schinkinger, S., Lincoln, B., Wottawah, F., Ebert, S., Romeyke, M., Lenz, D., Erickson, H.M., Ananthakrishnan, R., Mitchell, D., et al. (2005). Optical deformability as an inherent cell marker for testing malignant transformation and metastatic competence. Biophys. J. 88, 3689–3698. https://doi.org/10.1529/biophysj. 104.045476.
- 5. Xu, W., Mezencev, R., Kim, B., Wang, L., McDonald, J., and Sulchek, T. (2012). Cell
- stiffness is a biomarker of the metastatic potential of ovarian cancer cells. PLoS One 7, e46609. https://doi.org/10.1371/journal.pone.0046609.
- Luo, Q., Kuang, D., Zhang, B., and Song, G. (2016). Cell stiffness determined by atomic force microscopy and its correlation with cell motility. Biochim. Biophys. Acta 1860, 1953– 1960. https://doi.org/10.1016/j.bbagen.2016. 06.010.
- 7. Swaminathan, V., Mythreye, K., O'Brien, E.T., Berchuck, A., Blobe, G.C., and Superfine, R.



- (2011). Mechanical stiffness grades metastatic potential in patient tumor cells and in cancer cell lines. Cancer Res. 71, 5075–5080. https://doi.org/10.1158/0008-5472. CAN-11-0247.
- 8. Gawad, C., Koh, W., and Quake, S.R. (2016). Single-cell genome sequencing: current state of the science. Nat. Rev. Genet. 17, 175–188. https://doi.org/10.1038/nrg.2015.16.
- White, A.K., VanInsberghe, M., Petriv, O.I., Hamidi, M., Sikorski, D., Marra, M.A., Piret, J., Aparicio, S., and Hansen, C.L. (2011). Highthroughput microfluidic single-cell RT-qPCR. Proc. Natl. Acad. Sci. USA 108, 13999–14004. https://doi.org/10.1073/pnas.1019446108.
- Zhang, M., Matyunina, L.V., Walker, L.D., Chen, W., Xiao, H., Benigno, B.B., Wu, R., and McDonald, J.F. (2017). Evidence for the importance of post-transcriptional regulatory changes in ovarian cancer progression and the contribution of miRNAs. Sci. Rep. 7, 8171. https://doi.org/10.1038/s41598-017-08502-z.
- Maier, T., Güell, M., and Serrano, L. (2009). Correlation of mRNA and protein in complex biological samples. FEBS Lett. 583, 3966– 3973. https://doi.org/10.1016/j.febslet.2009. 10.036.
- Genshaft, A.S., Li, S., Gallant, C.J., Darmanis, S., Prakadan, S.M., Ziegler, C.G.K., Lundberg, M., Fredriksson, S., Hong, J., Regev, A., et al. (2016). Multiplexed, targeted profiling of single-cell proteomes and transcriptomes in a single reaction. Genome Biol. 17, 188. https://doi.org/10.1186/s13059-016-1045-6.
- Angermueller, C., Clark, S.J., Lee, H.J., Macaulay, I.C., Teng, M.J., Hu, T.X., Krueger, F., Smallwood, S., Ponting, C.P., Voet, T., et al. (2016). Parallel single-cell sequencing links transcriptional and epigenetic heterogeneity. Nat. Methods 13, 229–232. https://doi.org/10.1038/nmeth.3728.
- Cadwell, C.R., Palasantza, A., Jiang, X., Berens, P., Deng, Q., Yilmaz, M., Reimer, J., Shen, S., Bethge, M., Tolias, K.F., et al. (2016). Electrophysiological, transcriptomic and morphologic profiling of single neurons using Patch-seq. Nat. Biotechnol. 34, 199–203. https://doi.org/10.1038/nbt.3445.
- Kimmerling, R.J., Prakadan, S.M., Gupta, A.J., Calistri, N.L., Stevens, M.M., Olcum, S., Cermak, N., Drake, R.S., Pelton, K., De Smet, F., et al. (2018). Linking single-cell measurements of mass, growth rate, and gene expression. Genome Biol. 19, 207. https://doi.org/10.1186/s13059-018-1576-0.
- Mills, G.B., May, C., Hill, M., Campbell, S., Shaw, P., and Marks, A. (1990). Ascitic fluid from human ovarian cancer patients contains growth factors necessary for intraperitoneal growth of human ovarian adenocarcinoma cells. J. Clin. Invest. 86, 851–855. https://doi. org/10.1172/JCI114784.
- Matias-Guiu, J.A., Díaz-Álvarez, J., Ayala, J.L., Risco-Martín, J.L., Moreno-Ramos, T., Pytel, V., Matias-Guiu, J., Carreras, J.L., and Cabrera-Martín, M.N. (2018). Clustering analysis of FDG-PET imaging in primary progressive aphasia. Front. Aging Neurosci.

- 10, 230. https://doi.org/10.3389/fnagi.2018. 00230.
- Shao, M., Cao, L., Shen, C., Satpathy, M., Chelladurai, B., Bigsby, R.M., Nakshatri, H., and Matei, D. (2009). Epithelial-to-Mesenchymal transition and ovarian tumor progression induced by tissue transglutaminase. Cancer Res. 69, 9192–9201. https://doi.org/10.1158/0008-5472.CAN-09-1257.
- Liu, C.-Y., Lin, H.-H., Tang, M.-J., and Wang, Y.-K. (2015). Vimentin contributes to epithelial-mesenchymal transition cancer cell mechanics by mediating cytoskeletal organization and focal adhesion maturation. Oncotarget 6, 15966–15983.
- Nagaishi, M., Nakata, S., Ono, Y., Hirata, K., Tanaka, Y., Suzuki, K., Yokoo, H., and Hyodo, A. (2017). Tumoral and stromal expression of Slug, ZEB1, and ZEB2 in brain metastasis. J. Clin. Neurosci. 46, 124–128. https://doi. org/10.1016/j.jocn.2017.08.050.
- Spurlin, T.A., Bhadriraju, K., Chung, K.-H., Tona, A., and Plant, A.L. (2009). The treatment of collagen fibrils by tissue transglutaminase to promote vascular smooth muscle cell contractile signaling. Biomaterials 30, 5486– 5496. https://doi.org/10.1016/j.biomaterials. 2009.07.014.
- Lee, J., Condello, S., Yakubov, B., Emerson, R., Caperell-Grant, A., Hitomi, K., Xie, J., and Matei, D. (2015). Tissue transglutaminase mediated tumor-stroma interaction promotes pancreatic cancer progression. Clin. Cancer Res. 21, 4482–4493. https://doi. org/10.1158/1078-0432.CCR-15-0226.
- 23. Wei, S.C., Fattet, L., Tsai, J.H., Guo, Y., Pai, V.H., Majeski, H.E., Chen, A.C., Sah, R.L., Taylor, S.S., Engler, A.J., et al. (2015). Matrix stiffness drives Epithelial-Mesenchymal Transition and tumour metastasis through a TWIST1-G3BP2 mechanotransduction pathway. Nat. Cell Biol. 17, 678–688. https://doi.org/10.1038/ncb3157.
- Li, F., Cima, I., Vo, J.H., Tan, M.-H., and Ohl, C.D. (2020). Single cell hydrodynamic stretching and microsieve filtration reveal genetic, phenotypic and treatment-related links to cellular deformability. Micromachines 11, 486. https://doi.org/10.3390/mi11050486.
- Qi, D., Kaur Gill, N., Santiskulvong, C., Sifuentes, J., Dorigo, O., Rao, J., Taylor-Harding, B., Ruprecht Wiedemeyer, W., and Rowat, A.C. (2015). Screening cell mechanotype by parallel microfiltration. Sci. Rep. 5, 17595. https://doi.org/10.1038/ srep17595.
- Irianto, J., Pfeifer, C.R., Ivanovska, I.L., Swift, J., and Discher, D.E. (2016). Nuclear lamins in cancer. Cell. Mol. Bioeng. 9, 258–267. https:// doi.org/10.1007/s12195-016-0437-8.
- Sreenivasappa, H., Chaki, S.P., Lim, S.-M., Trzeciakowski, J.P., Davidson, M.W., Rivera, G.M., and Trache, A. (2014). Selective regulation of cytoskeletal tension and cell– matrix adhesion by RhoA and Src. Integr. Biol. 6, 743–754. https://doi.org/10.1039/ c4ib00019f.

- Rao, G., Pierobon, M., Kim, I.-K., Hsu, W.-H., Deng, J., Moon, Y.-W., Petricoin, E.F., Zhang, Y.-W., Wang, Y., and Giaccone, G. (2017). Inhibition of AKT1 signaling promotes invasion and metastasis of non-small cell lung cancer cells with K-RAS or EGFR mutations. Sci. Rep. 7, 7066. https://doi.org/10.1038/ s41598-017-06128-9.
- Cheung, K.J., Gabrielson, E., Werb, Z., and Ewald, A.J. (2013). Collective invasion in breast cancer requires a conserved basal epithelial program. Cell 155, 1639–1651. https://doi.org/10.1016/j.cell.2013.11.029.
- Konen, J., Summerbell, E., Dwivedi, B., Galior, K., Hou, Y., Rusnak, L., Chen, A., Saltz, J., Zhou, W., Boise, L.H., et al. (2017). Imageguided genomics of phenotypically heterogeneous populations reveals vascular signalling during symbiotic collective cancer invasion. Nat. Commun. 8, 15078. https://doi. org/10.1038/ncomms15078.
- 31. Hapach, L.A., Carey, S.P., Schwager, S.C., Taufalele, P.V., Wang, W., Mosier, J.A., Ortiz-Otero, N., McArdle, T.J., Goldblatt, Z.E., Lampi, M.C., et al. (2021). Phenotypic heterogeneity and metastasis of breast cancer cells. Cancer Res. 81, 3649–3663. https://doi.org/10.1158/0008-5472.CAN-20-1799.
- Islam, M., Mezencev, R., McFarland, B., Brink, H., Campbell, B., Tasadduq, B., Waller, E.K., Lam, W., Alexeev, A., and Sulchek, T. (2018). Microfluidic cell sorting by stiffness to examine heterogenic responses of cancer cells to chemotherapy. Cell Death Dis. 9, 239. https://doi.org/10.1038/s41419-018-0266-x.
- 33. Chernaya, O., Zhurikhina, A., Hladyshau, S., Pilcher, W., Young, K.M., Ortner, J., Andra, V., Sulchek, T.A., and Tsygankov, D. (2018). Biomechanics of endothelial tubule formation differentially modulated by cerebral cavernous malformation proteins. iScience 9, 347–358. https://doi.org/10.1016/j.isci.2018.11.001.
- Ni, F., Yu, W.-M., Wang, X., Fay, M.E., Young, K.M., Qiu, Y., Lam, W.A., Sulchek, T.A., Cheng, T., Scadden, D.T., and Qu, C.K. (2019). Ptpn21 controls hematopoietic stem cell homeostasis and biomechanics. Cell Stem Cell 24, 608–620.e6. https://doi.org/10.1016/j.stem.2019.02.009.
- Bongiorno, T., Gura, J., Talwar, P., Chambers, D., Young, K.M., Arafat, D., Wang, G., Jackson-Holmes, E.L., Qiu, P., McDevitt, T.C., and Sulchek, T. (2018). Biophysical subsets of embryonic stem cells display distinct phenotypic and morphological signatures. PLoS One 13, e0192631. https://doi.org/10. 1371/journal.pone.0192631.
- Schindelin, J., Arganda-Carreras, I., Frise, E., Kaynig, V., Longair, M., Pietzsch, T., and Cardona, A. (2012). Fiji: an open-source platform for biological-image analysis. Nat. Methods 9, 676–682.
- 37. Untergasser, A., Ruijter, J.M., Benes, V., and van den Hoff, M.J. (2021). Web-based LinRegPCR: application for the visualization and analysis of (RT)-qPCR amplification and melting data. BMC Bioinformatics 22, 398.



- Haase, K., and Pelling, A.E. (2015). Investigating cell mechanics with atomic force microscopy. J. R. Soc. Interface 12, 20140970. https://doi.org/10.1098/rsif. 2014.0970.
- Moreno-Flores, S., Benitez, R., Vivanco, M.d., and Toca-Herrera, J.L. (2010). Stress relaxation and creep on living cells with the atomic force microscope: a means to calculate elastic moduli and viscosities of cell components. Nanotechnology 21, 445101. https://doi.org/10.1088/0957-4484/21/44/ 445101.
- Cheon, D.-J., Tong, Y., Sim, M.-S., Dering, J., Berel, D., Cui, X., Lester, J., Beach, J.A., Tighiouart, M., Walts, A.E., et al. (2014). A collagen-remodeling gene signature regulated by TGF-β signaling is associated with metastasis and poor survival in serous ovarian cancer. Clin. Cancer Res. 20, 711–723. https://doi.org/10.1158/1078-0432.CCR-13-1256.
- 41. Foster, R., Buckanovich, R.J., and Rueda, B.R. (2013). Ovarian cancer stem cells: working

- towards the root of stemness. Cancer Lett. 338, 147–157. https://doi.org/10.1016/j. canlet.2012.10.023.
- Cheaib, B., Auguste, A., and Leary, A. (2015). The PI3K/Akt/mTOR pathway in ovarian cancer: therapeutic opportunities and challenges. Chin. J. Cancer 34, 4–16. https:// doi.org/10.5732/cjc.014.10289.
- Lawson, D.A., Bhakta, N.R., Kessenbrock, K., Prummel, K.D., Yu, Y., Takai, K., Zhou, A., Eyob, H., Balakrishnan, S., Wang, C.-Y., et al. (2015). Single-cell analysis reveals a stem-cell program in human metastatic breast cancer cells. Nature 526, 131–135.
- Fife, C.M., McCarroll, J.A., and Kavallaris, M. (2014). Movers and shakers: cell cytoskeleton in cancer metastasis. Br. J. Pharmacol. 171, 5507–5523. https://doi.org/10.1111/bph. 12704.
- Dupont, S., Morsut, L., Aragona, M., Enzo, E., Giulitti, S., Cordenonsi, M., Zanconato, F., Le Digabel, J., Forcato, M., Bicciato, S., et al. (2011). Role of YAP/TAZ in

- mechanotransduction. Nature 474, 179–183. https://doi.org/10.1038/nature10137.
- Wu, Z., Wu, L., Weng, D., Xu, D., Geng, J., and Zhao, F. (2009). Reduced expression of lamin A/C correlates with poor histological differentiation and prognosis in primary gastric carcinoma. J. Exp. Clin. Cancer Res. 28, 8. https://doi.org/10.1186/1756-9966-28-8.
- Mezencev, R., Matyunina, L.V., Jabbari, N., and McDonald, J.F. (2016). Snail-induced epithelial-to-mesenchymal transition of MCF-7 breast cancer cells: systems analysis of molecular changes and their effect on radiation and drug sensitivity. BMC Cancer 16, 236. https://doi.org/10.1186/s12885-016-2274-5.
- Davies, D.L., and Bouldin, D.W. (1979). A cluster separation measure. IEEE trans. Pattern anal. Mach. Intell. IEEE Trans. Pattern Anal. Mach. Intell. 1, 224–227. https://doi. org/10.1109/tpami.1979.4766909.





STAR*METHODS

KEY RESOURCES TABLE

REAGENT or RESOURCE	SOURCE	IDENTIFIER
Chemicals, peptides, and recombinant proteins		
0.1% gelatin in sterile water	Fisher Scientific	Cat#ES006B
CellsDirect™ One-Step qRT-PCR Kit - 2x reaction mix	ThermoFisher	Cat#11753-100
SUPERase inhibitor	ThermoFisher	Cat#AM2694
SsoAdvanced™ Universal SYBR® Green Supermix	BioRad	Cat#1725271
SsoFastTM EvaGreen® SuperMix with Low ROX	BioRad	Cat#172-5211
Exonuclease I	New England BioLabs	Cat#M0293S
CellsDirect™ One-Step qRT-PCR Kit - Super-Script III RT Platinum Taq Mix	ThermoFisher	Cat#11753-100
Critical commercial assays		
CytoSelect™ Cell Migration (Chemotaxis) Assay Kits, 8 µm Pore Size, Cell Biolabs	Cell BioLabs	Cat#CBA-101
Deposited data		
Single cell gene expression and phenotype dataset	This paper	GSE154031, https://www.ncbi.nlm.nih.gov/geo/query/acc.cgi?acc=GSE154031
Experimental models: Cell lines		
HEY ovarian cancer cell line	Dr. John McDonald	RRID:CVCL_0297
HEY A8 ovarian cancer cell line	Dr. John McDonald	RRID:CVCL_8878
OVCAR3 ovarian cancer cell line	Dr. John McDonald	RRID:CVCL_0465
Oligonucleotides		
PCR Primers	See Table S2	N/A
Software and algorithms		
Rasylum: Custom R code for AFM force curve analysis	This paper	https://doi.org/10.5281/zenodo.7023891
ThesisCode: Custom R code for analyzing qPCR data from Fluidigm BioMark system	This paper	https://doi.org/10.5281/zenodo.7023900
Fiji: Fiji is Just ImageJ - Image processing software	Schindelinet al., 2012 ³⁶	https://doi.org/10.1038/nmeth.2019
LinRegPCR: RT-qPCR analysis software	Untergasser et al., 2021 ³⁷	https://doi.org/10.1186/s12859-021-04306-1

RESOURCE AVAILABILITY

Lead contact

Further information and requests for resources and reagents should be directed to and will be fulfilled by the lead contact, Todd Sulchek (todd.sulchek@me.gatech.edu).

Materials availability

This study did not generate new unique reagents.

Data and code availability

- The datasets generated and analyzed during the current study are available from the corresponding author on reasonable request. The gene expression dataset supporting the conclusions of this article has been deposited in the NCBI Gene Expression Omnibus (GEO) repository and is publicly available as of the date of publication. Accession numbers are listed in the key resources table.
- All original code has been deposited on GitHub and archived using Zenodo; it is publicly available as of the date of publication. DOIs are listed in the key resources table.



 Any additional information required to reanalyze the data reported in this paper is available from the lead contact upon request.

EXPERIMENTAL MODEL AND SUBJECT DETAILS

Ovarian cell culture and sample preparation

The mesenchymal female ovarian cancer cell line HEY (RRID:CVCL_0297) and its derivative cell line HEY A8 (RRID:CVCL_8878) were cultured in RPMI-1640 media (Sigma-Aldrich) supplemented with 10% fetal bovine serum (Atlanta Biologicals) and 1% penicillin-streptomycin (Sigma-Aldrich). The epithelial female ovarian cancer cell line OVCAR3 (RRID:CVCL_0465) was cultured in RPMI-1640 media supplemented with 20% fetal bovine serum and 1% penicillin-streptomycin. Cells were cultured at 37 °Cat 5% CO $_2$. All three cell lines were provided by Dr. John McDonald. All three cell lines were submitted to ATCC for STR profiling and there was a match between all three submitted reads with their respective database profiles. The day before AFM experiments, 10,000 cells were seeded on a gelatin-coated (Fisher Scientific) gridded coverslip (Electron Microscopy Sciences) in 24-well plates.

METHOD DETAILS

AFM and force curve analysis

For better global stiffness measurements of the cell, 5.46 μ m spherical polystyrene particles were attached to tipless silica nitride cantilevers (Bruker Probes) using a two-part epoxy. To characterize the mechanical properties of each cell, we used force spectroscopy to obtain force-indentation curves with an atomic force microscope (Asylum Research) with an integrated optical microscope (Nikon) on a vibration isolation table. Before each day of measurements, each cantilever was calibrated to determine the deflection inverse optical lever sensitivity and spring constant (k is approximately 10–25 pN/nm). For measurements, the cantilever probe was visually aligned with the cell center and moved with a velocity of 2 μ m/s to indent the cell with increasing compressive force until a force trigger of 10 nN was reached. The cantilever was held in position for 5 seconds, dwelling towards the surface, allowing for viscous relaxation of the cell before reversing the direction of its velocity.

We used custom code written in R (https://github.com/nstone8/Rasylum) relying on the Hertzian contact model, which describes non-adhesive elastic contact between two bodies, to calculate the cellular reduced Young's modulus. ³⁸ The contact point was estimated by the intersection of the flat, undeformed region of the force curve with a line fit to the force curve region where the cantilever was in contact with the cell. Next, we identified the true contact point by iteratively testing the points around the estimated contact point with the minimal residual difference between the measured force curve and a nonlinear fit described by the governing equation Hertz used to describe the contact between an elastic sphere and an elastic half space. We additionally used custom R code to fit the dwell region of the force curve to a biexponential decay curve to identify the fast and slow viscous time constants.³⁹

Image analysis

For every cell mechanically probed, we additionally captured an optical microscopy image to be analyzed for size and various shape descriptors using ImageJ software. Each cell was outlined, and its area was measured. This outline was then fit with an ellipse to determine the major and minor axis of each cell. We use four shape descriptors to describe each cell: the aspect ratio (the ratio of the major axis to the minor axis), circularity $(4\pi^*$ area/perimeter²), roundness $(4^*$ area/ $(\pi^*$ major axis²)) and solidity (area/convex area).

Micropipette isolation

After approximately 40 minutes of AFM measurements, the coverslip with the cells attached was moved to a micropipette rig for aspiration. Micropipettes were pulled from borosilicate standard wall glass capillaries (1.5 mm OD, 0.86 mm ID, Warner Instruments) using a PC-10 vertical puller (Narishige) producing pipettes with an opening diameter of approximately 6.5 μ m. Due to the sensitivity of single cell gene expression techniques, caution was exercised in the decontamination of the system along with the removal of all RNAse and DNAse enzymes. Using micromanipulators (Scientifica) to control the x-y-z position of the micropipette, the micropipette tip was located with a 40x objective light microscope and lowered to each cell of interest. Once together, 345 to 500 mbar of negative pressure was applied for 0.2 to 2 seconds to aspirate the cell of interest into the micropipette. The micropipette was then removed from the bath and 1000 mbar of positive pressure was applied for 3 seconds to displace the aspirated cell into an individual





PCR tube containing 5 μ L of CellsDirect One-Step qRT-PCR 2x reaction mix (Invitrogen) with 1 U/ μ L of SUPERase-In, a RNAse inhibitor (Ambion). In general, there was approximately 1-2 hours between mechanical measurements and isolation of each cell. These individual cells were stored at -80°C.

Fluorescent activated cell sorting (FACS)

To compare micropipette isolation with FACS single cell isolation, HEY A8 cells were resuspended to 1 \times 10⁶ cells/mL in a sorting buffer (PBS + 1% FBS + 1 mM EDTA + 25 mM HEPES) and sorted using a FACS Aria IIIu Cell Sorter (Becton Dickinson) into a PCR plate containing 5 μ L of CellsDirect One-Step qRT-PCR 2x reaction mix (Invitrogen) with 1 U/ μ L of SUPERase-In, a RNAse inhibitor (Ambion) in each well. Cells were gated based on forward and side scatter to select living, single cells.

Primer design and validation

A list of genes of interest was curated from various published sources and experimental comparisons of gene expression between cell lines of varying metastatic potential. 40–47 Designs for these 96 genes of interest were collected from previously published studies, choosing primer sets predicted by the Basic Local Alignment Search Tool (BLAST). We validated each primer set (ThermoFisher) using qPCR with SsoAdvanced Universal SYBR Green Supermix (BioRad) and cDNA reverse transcribed from mRNA extracted and purified from HEY, HEY A8 and OVCAR3 cells. We then analyzed each PCR product on gel electrophoresis to confirm the expected product size. There were 90 primer sets that produced the correct single PCR product.

Fluidigm targeted qPCR

We followed the advanced development protocol from Fluidigm for investigating single cell gene expression using SsoFast EvaGreen with Low ROX on the BioMark system (Fluidigm, ADP 41). Super-Script III RT Platinum Taq Mix (Invitrogen) and a mix of 500 nM of all forward and reverse primers was added to the single cells stored in the reaction mix for reverse transcription and specific target amplification. To clean up unincorporated primers, we included an Exonuclease I (New England BioLabs) digestion. Amplified single cell samples were combined with SsoFast EvaGreen Supermix with Low ROX (BioRad) and DNA Binding Dye (Fluidigm) and each primer pair was diluted and combined with an assay-loading reagent (Fluidigm). The 96.96 Dynamic Array integrated fluidic chip (Fluidigm) was loaded with 96 samples (including a positive and negative control) and 96 assays with the IFC Controller HX (Fluidigm). Using a BioMark machine (Fluidigm), we performed 40 cycles of PCR and a melt curve analysis.

Raw data was exported from the Fluidigm Real-Time PCR Analysis Software. R code (https://github.com/kyoung74/ThesisCode) was used to calculate R_n values at each cycle number for each sample and assay combination by taking the ratio of the difference between the raw and background EvaGreen fluorescence readings and the difference between the raw and background ROX fluorescence readings. These R_n values were then analyzed using LinRegPCR (https://www.medischebiologie.nl/files/) to determine a C_t for each sample-assay pair. We transformed this C_t value by subtracting it from 45. Additionally, we identified GAPDH and RPL32 as stable housekeeping genes in our 3 cell types and removed single cell samples where either of these housekeeping genes did not amplify. The transformed C_t values were normalized to the geometric mean of the GAPDH and RPL32 expression and cells where the normalized GAPDH expression was lower than 0.8 were also removed.

Population gene expression qPCR

To compare the gene expression of each cell line population, we used qPCR with SsoAdvanced Universal SYBR Green Supermix (BioRad) and cDNA reverse transcribed from mRNA extracted and purified from T-25 flasks of HEY, HEY A8 and OVCAR3 cells (approximately 2 million cells each). Amplification curves from the ABI StepOne Plus qPCR machine were analyzed using LinRegPCR (https://www.medischebiologie.nl/files/) to determine a C_t for each sample-assay pair. We transformed this C_t value by subtracting it from 45. The transformed C_t values were normalized to the geometric mean of the *GAPDH* and *RPL32* expression. The micropipette-isolated single cell values of normalized expression of each gene for each cell type was averaged and plotted against the population gene expression. A Pearson's correlation test was used to compare the population and average single cell gene expression.



Migration assay

To test the migratory properties of each cell type (Figure 3A), we used the CytoSelect 96-well transwell migration assay (Cell BioLabs), where 50,000 cells of each cell population were seeded in serum free media (DMEM media supplemented with 0.5% BSA, 2 mM CaCl₂, 2 mM MgCl₂, and 1% penicillin-streptomycin) in an 8-micron pore well insert, leading to a well filled with complete media (RPM1-1640 media supplemented with 10% FBS and 1% penicillin-streptomycin). After 8 hours of incubation, cells that migrated through the pores and were detached, lysed and fluorometrically dyed with CyQuant GR fluorescent dye. The amount of fluorescence per well was read with a plate reader at 480 nm/520 nm (BioTek).

All assays were carried out in biological triplicate with an initial time course study conducted to ascertain at which time there was significant transmigration of cells.

siRNA transfection

For testing the role of SRC and TGM2 in cell stiffness, HEY A8 and OVCAR3 cells were seeded one day before transfection (125,000 cells per T25 and 25,000 cells per FluoroDish (World Precision Instruments)). A transfection mixture of equal parts diluted siRNA (33 μ L of 10 μ M siRNA + 217 μ L serum free media) and diluted Lipofectamine RNAiMAX transfection reagent (ThermoFisher) (17 μ L of TR in 233 μ L of serum free media). After a 5 minute incubation at room temperature, 250 uL of the mixture was added to 5 mL of media without antibiotics. After 48 hours, the RNA was extracted and tested with RT-qPCR and AFM was used to measure the effect of SRC and TGM2 on cell stiffness.

QUANTIFICATION AND STATISTICAL ANALYSIS

PCA and PLS cell clustering analysis

First, we separately transformed the normalized gene expression data, the morphological measurements, and the mechanical data of all single cells using principal component analysis (PCA). Then we applied partial least squares (PLS) analysis to combine gene expression data with morphological and mechanical measurements followed by PCA to cluster cells based on the combination of two or three data types. We quantified the clustering results using the Davies-Bouldin index (DB index), ⁴⁸ which characterizes the ratio of variance of data points in the same cluster and the variance of data points between clusters. After using PLS to combine the different data types, we selected the number of PLS components for each combination that minimized the DB index which indicates the most optimal clustering algorithm (4 PLS components for mechanical and morphological data, 3 PLS components for gene expression and morphological data, 7 PLS components for gene expression and mechanical data, and 8 PLS components for gene expression, morphological and mechanical data).

Correlation analysis

With the normalized gene expression of the 85 validated, non-housekeeping genes, 3 mechanical parameters and 7 morphological parameters from the single cells from all three cell lines, we used Spearman's correlation analysis to investigate the pairwise correlation between all combinations of the 95 parameters and the significance of each correlation (p < 0.05 considered significant). This analysis was repeated using the single cell data from each cell line separately. Literature review was used to identify the function of each gene of interest as well as its expected effect on cancer metastasis.